Characterizing nonlinear piezoelectric dynamics through deep neural operator learning

Chandra, Abhishek; Kapoor, Taniya; Curti, Mitrofan; Tiels, Koen; Lomonova, Elena A.

Characterizing nonlinear piezoelectric dynamics through deep neural operator learning

Abhishek Chandra,[1,2,a] (iD) Taniya Kapoor,[3] (iD) Mitrofan Curti,[1,2] (iD) Koen Tiels,[2,4] (iD) and Elena A. Lomonova[1,2] (iD)

AFFILIATIONS

[1]Electromechanics and Power Electronics Group, Department of Electrical Engineering, Eindhoven University of Technology, 5600 MB Eindhoven, The Netherlands
[2]Eindhoven Artificial Intelligence Systems Institute, Eindhoven University of Technology, 5612 AP Eindhoven, The Netherlands
[3]Department of Engineering Structures, Delft University of Technology, 2628 CN Delft, The Netherlands
[4]Control Systems Technology Group, Department of Mechanical Engineering, Eindhoven University of Technology, 5600 MB Eindhoven, The Netherlands

[a]Author to whom correspondence should be addressed: a.chandra@tue.nl

ABSTRACT

Nonlinear hysteresis modeling is essential for estimating, controlling, and characterizing the behavior of piezoelectric material-based devices. However, current deep-learning approaches face challenges in generalizing effectively to previously unseen voltage profiles. This Letter tackles the limitation of generalization by introducing the notion of neural operators for modeling the nonlinear constitutive laws governing inverse piezoelectric hysteresis, specifically focusing on the relationship between voltage inputs and displacement responses. The study utilizes two neural operators—Fourier neural operator and the deep operator network—to predict material responses to unseen voltage profiles that are not part of the training data. Numerical experiments, including butterfly-shaped hysteresis curves, show that in accuracy and generalization to unseen voltage profiles, neural operators outperform traditional recurrent neural network-based models, including conventional gated networks. The findings highlight the potential of neural operators for modeling hysteresis in piezoelectric materials, offering advantages over existing methods in varying voltage scenarios.

Piezoelectric materials are functional materials that correspond to electrical and mechanical energy interactions.[1] Prominently characterized by two types of dynamics, piezoelectric dynamics corresponds to the action where an applied mechanical stress on the material induces a voltage, and inverse piezoelectric dynamics, where the applied electrical energy leads to a mechanical displacement. The dynamics are typically nonlinear and characterized by memory effects, depending on past input states that lead to hysteresis.[2] Hence, precise hysteresis modeling is essential for optimal control and characterization of piezoelectric material-based devices.[3]

The focus of this Letter is to model the inverse piezoelectric hysteresis, which is to model the voltage–displacement relationship. The relationship between voltage and displacement is nonlinear and dependent on previous system states, exhibiting history dependence. Traditionally, phenomenological models, such as the Preisach model,[4] are employed to model this relationship. However, the Preisach model requires certain specific measurement samples, like the first-order

reversal curves, to characterize the materials.[5] Due to these stringent restrictions and cheap inference cost of trained deep learning models compared to the Preisach model,[6–8] neural networks are increasingly being utilized to model piezoelectric hysteresis.[9]

The history-dependent characteristics of hysteresis lead to a conceptual overlap with the recurrent neural network domain.[10] Owing to this overlap, recurrent architecture-based methods have been applied to model hysteresis for piezoelectric materials and devices.[11,12] As a natural framework, advanced recurrent networks have been widely used to model hysteresis, such as long short-term memory (LSTM)[13] based and gated recurrent unit (GRU)[14] based approaches.[2,15–17]

However, an important aspect of modeling a piezoelectric material or a device is predicting the material's response to unseen voltage inputs that are not used to train the neural network model. In this regard, the recurrent models face challenges in generalizing[18–21] the trained model to adapt to unseen input signals and predicting the voltage–displacement dynamics, as shown in this Letter. A possible reason

for such a failure is the functional relationship learned between the voltage and displacement profiles, which is largely data-driven and fails to capture the inherent dynamic trend between the input and the output in general.[22]

Learning a neural network-based model to predict output displacement fields given any input voltage refers to learning a functional map from voltage functional space to displacement functional space. If learned, such a mapping would facilitate predicting the displacements for unseen voltage profiles, leading to a generalized neural network-based model for learning and predicting piezoelectric dynamics. Such a model could be used offline for downstream tasks to predict unseen scenarios in real-time,[23] facilitating applications such as control.

Neural operators[24,25] are a class of supervised deep learning models that map input and output function spaces using the observed data as discussed in a recent review paper.[23] Neural operators have been used for physical simulations,[26,27] and for modeling in different domains, for instance, lithium-ion batteries,[28] multiscale mechanics,[29] and magnetic materials.[22] However, it is unexplored for modeling the hysteresis behavior of piezoelectric materials.

The contributions of the current work are as follows: this Letter proposes an approach shift in modeling the nonlinear hysteretic relationship prevalent in piezoelectric materials through neural operators. The neural operator strategy exhibits advantages compared to the recurrent architectures such as LSTM and GRU through experiments on hysteresis loops, including butterfly-shaped hysteresis. More broadly, this Letter bridges the gap between scientific machine learning and piezoelectric hysteresis modeling, which could be used widely due to low inference times and high accuracy and generalization abilities.[23]

The rest of the letter describes the method employed to model the hysteresis, particularly the neural operator architectures and specifics of the Fourier neural operator (FNO)[24] and the deep operator network (DeepONet)[25] and their corresponding training details. Subsequently, the method is employed to model hysteresis, including the butterfly-shaped hysteresis, and compared with recurrent models like LSTM and GRU. Finally, the results are discussed, and conclusions and future works are collated regarding the conducted study.

The motivation to employ neural operators corresponds to the necessity of generalizable models predicting displacements for different and unseen voltage profiles. A vanilla function approximator, such as a deep neural network, maps the measured ordered data pairs for voltages (v) and displacement (d), that is (v_i, d_i), for $1 \leq i \leq N$, $i \in \mathbb{Z}$ for N observations. A deep neural network $\mathcal{N}(\theta)$, parameterized by learnable parameters θ, aims to approximate the relationship between v_i and d_i through a function f, such that $d_i \approx f(v_i)$. However, such learning does not generalize to unseen sequences of the voltage profiles, posing challenges for a neural network model to take an arbitrary v sequence from a functional space as input and map it to the corresponding d sequence.[22] Learning such a map would facilitate predicting displacement for any unseen voltage profile from the functional space.

The required dataset to train the neural operators consists of first sampling n_{func} number of input v functions from an appropriate functional space. The choice of the functional space depends on the particular application and assumptions of the material for which the modeling is performed and the assumptions regarding the voltage profiles expected to be applied to the material. For our experiments, the voltage profiles are generated from the sinusoidal spaces. After

generating from the sinusoidal spaces, the voltage profiles are applied to the material or a surrogate material model to generate the data pairs. The surrogate models in this Letter are solely used to explore the necessary functional spaces to generate the data. To characterize the material in practice, voltage profiles should be applied to the material in a physical experiment. Subsequently, the dataset (v_i, d_i) is stored for all n_{func} functions along with the time locations array t on which the functions are sampled.

The first neural operator employed in this work is the Fourier neural operator (FNO), which thrives on convolutional neural network architecture, as shown in Fig. 1. The inputs for FNO are the normalized[30] voltage fields v_i concatenated with the time array by repeating it sufficiently to form the input tensor $X := [v_i, t]$ of channel size two. The input X is further projected through a tensor, P, increasing the number of channels to N_f, i.e., $z^0 = PX$. The tensor z^0 is subsequently processed through a series of Fourier layers, which are parameterized by learnable tensors W and R. The operations within these Fourier layers can be represented as follows:

$$z^{l+1} = \sigma(W^l z^l + \mathcal{F}^{-1}(R^l \mathcal{F}(z^l))), \quad (1)$$

where z^l represents the latent tensor at the lth layer. The method first applies a fast Fourier transform (FFT), denoted by $\mathcal{F}$. The first n_m modes are then subjected to a linear transformation using $R \in \mathbb{C}^{\mathcal{F}_{\text{out}} \times \mathcal{F}_{\text{out}}}$, followed by an inverse FFT, $\mathcal{F}^{-1}$. Here, $\mathcal{F}_{\text{out}}$ indicates the dimensionality of $\mathcal{F}(z^l)$. The resulting tensor is combined with a linearly transformed latent tensor $W^l z^l$. A nonlinear activation function, σ, is subsequently applied to yield z^{l+1}. This sequence of operations is repeated across L Fourier blocks. The output from the final Fourier block, z^L, is downscaled via two projection tensors, Q and $\widehat{Q}$, to produce the predicted displacements $\widehat{d}_i$ as follows:

$$\widehat{d}_i = \widehat{Q}\sigma(Q z^L). \quad (2)$$

The mean square loss function for FNO is

$$L(\theta) = \frac{1}{N} \sum_{i=1}^{N} (\widehat{d}_i(\theta) - d_i)^2. \quad (3)$$

The network parameters θ are obtained using a gradient-based optimization technique. Alternative loss functions that minimize the residual using different norms can also be considered.

The second neural operator utilized in this study is the deep operator network—DeepONet. The standard DeepONet architecture[25] is based on fully connected feedforward neural networks, illustrated in
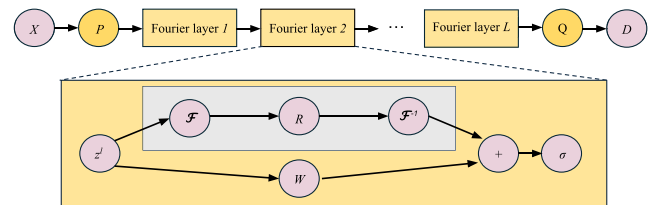

FIG. 1. Neural architecture for Fourier neural operator (FNO). The input $X := [v, t]$ is passed through projection tensor (P) and Fourier layers and finally downscaled (Q) to approximate the displacement.
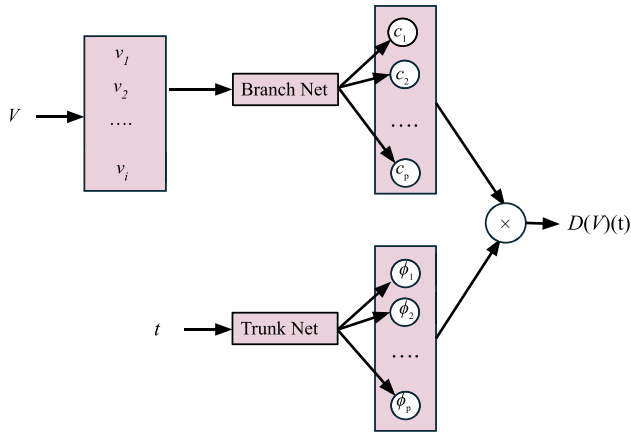
FIG. 2. Deep Operator Network (DeepONet) architecture comprising two independent feedforward neural networks—the branch net and the trunk net—whose outputs are combined through a dot product to approximate the displacement.

Fig. 2. The architecture consists of two distinct feedforward neural networks: the branch net and the trunk net. In this work, the branch net processes functions from the input voltage functional space, specifically the training fields v_i from the V space. The trunk net takes an array, t, where the output fields are evaluated. The branch and trunk networks are structured with hidden layers and output neurons, similar to conventional feedforward networks.

While the number of hidden layers in the branch and trunk networks can vary, the number of output neurons must be identical in both nets. This requirement is essential for their outputs to be combined through a dot product operation to approximate the displacements d_i as $\widehat{d}_i$ in the displacement functional space D. Mathematically, this approximation is expressed as $d_i \approx \widehat{d}_i = \sum_{k=1}^{p} c_k \phi_k$, where c_k are the outputs of the branch net, and ϕ_k are the outputs of the trunk net. From the perspective of traditional function approximation, ϕ_k can be interpreted as basis functions, with c_k serving as their coefficients, combined over p terms to approximate the field d_i. The same loss function as in the FNO case, given by (3), is applied to approximate d_i.

The presented numerical experiments aim to model the hysteresis loop between the voltage and the displacement. The data for the experiment are generated by simulating the Bouc–Wen models[31] using the `odeint` module of the `scipy` package. For the first experiment, the considered Bouc–Wen ordinary differential equation (ODE) is

$$\dot{d}(t) = 0.4|\dot{v}(t)|v(t) - 0.85|\dot{v}(t)|d(t) + 0.25\dot{v}(t), \quad (4)$$

with the initial condition $d(0) = 0$. Here, $d(t)$ and $v(t)$ denote the displacement and voltage at time t, respectively, and $\dot{x}$ refers to the derivative of the quantity x. For $N = 100$ equidistant times in the domain $t \in [0, 1]$, a total of $n_{\text{func}} = 2000$ voltage profiles are sampled by varying the amplitudes randomly. A sine function with a fixed frequency is computed for each amplitude over 100 equally spaced time arrays. Out of the 2000 samples, 1000 are taken to train the model, and randomly, the model is tested for another 1000 functions. The error in approximating the displacement sequences d as $\widehat{d}$ by the neural networks is averaged over all 1000 test samples and computed through three error metrics: relative error in L^2 norm ($\mathscr{R}$), mean absolute error (MAE),

and root mean square error (RMSE). The metrics are defined as follows:

$$\mathscr{R} = \frac{\sqrt{\frac{1}{1000}\sum_{j=1}^{1000}(\widehat{d}_j - d_j)^2}}{\sqrt{\frac{1}{1000}\sum_{j=1}^{1000}d_j^2}}, \quad (5)$$

$$\text{MAE} = \frac{1}{1000}\sum_{j=1}^{1000}|\widehat{d}_j - d_j|, \quad (6)$$

$$\text{RMSE} = \sqrt{\frac{1}{1000}\sum_{j=1}^{1000}(\widehat{d}_j - d_j)^2}. \quad (7)$$

First, FNO is employed to model the voltage–displacement hysteresis relationship given by (4). The network consists of a fully connected layer to lift the dimension from 2 channels to 8 channels, i.e., $N_f = 8$. This lifting is followed by four spectral convolutional layers ($L = 4$), each consisting of eight input and output channels. The first four modes ($n_m = 4$) are retained for each block after the Fourier transformation. The network projects back to the physical space using two fully connected layers, transforming dimensions from 8 channels to 128 and finally to a single output channel. The complete architecture employs the ReLU activation function. A batch size of 100 samples over 500 epochs is employed consistently, utilizing the ADAM optimizer[32] with a learning rate of 1×10^{-3}.

Further, DeepONet is employed to predict the hysteresis loops. DeepONet takes as input for the branch net 1000 random voltage fields and the t array of size 100 for the trunk net. The branch and trunk nets are based on fully connected feedforward neural networks, with five hidden layers with 40 neurons in each layer and a tanh activation function. The output dimension of $p = 100$ is kept for the branch and trunk nets. Xavier initialization[33] is used to initialize the model parameters, and the network is trained using the ADAM optimizer over 20 000 epochs with a learning rate of 5×10^{-5}.

The results depicting the performance of FNO and DeepONet are presented in Fig. 3. The input voltage profiles for training and testing are shown in Fig. 3(a) with blue and red curves, respectively. The results demonstrate that FNO and DeepONet exhibit generalizable performance in approximating the hysteresis loops and capturing the relationship between voltage and displacement for the piezoelectric material. FNO, as illustrated in Fig. 3(b), shows an accuracy close to the eye-ball norm in capturing the nonlinear characteristics of the hysteresis loops. The predicted curves (solid black) align closely with the ground truth (dashed red), suggesting that FNO effectively learns and generalizes the system's underlying physical dynamics.

Similarly, DeepONet, shown in Fig. 3(c), demonstrates strong performance, albeit with slightly less precision than FNO. The alignment between the predicted curves and the ground truth remains close, although there are minor deviations in the amplitude and phase of the predicted loops. The overall trend suggests that DeepONet can model the voltage–displacement relationship, showcasing its ability to learn continuous operators.

The neural operators are compared with LSTM and GRU, owing to their potential in modeling the time-dependent relationships. LSTM and GRU predictions depicted in Figs. 3(d) and 3(e) fail to capture the hysteresis behavior accurately. The predictions generated by LSTM and GRU exhibit significant discrepancies compared to the ground truth. Specifically, the LSTM predictions, as shown in Fig. 3(d), display
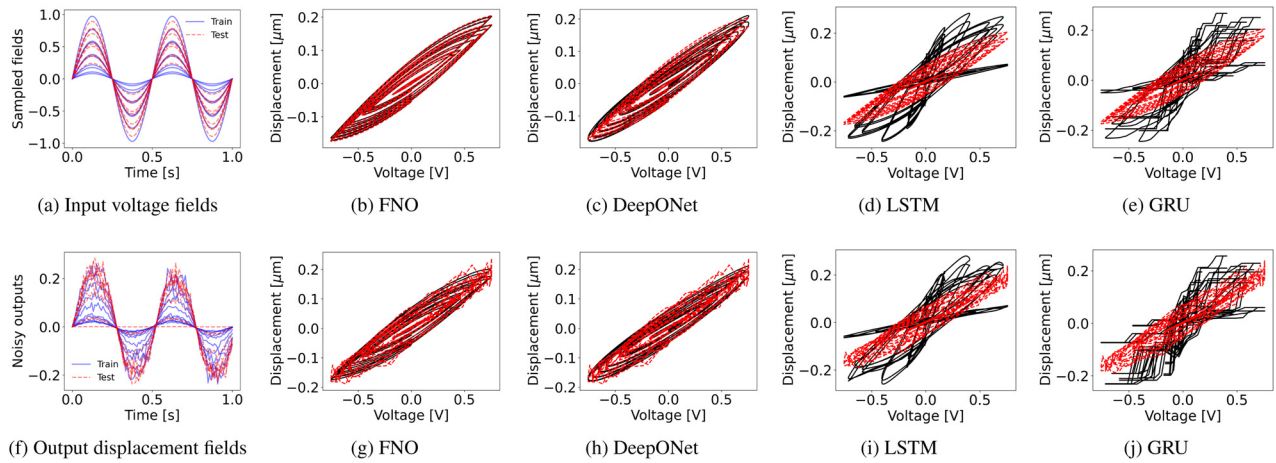
FIG. 3. Performance of neural network models in predicting hysteresis loops described by (4) for sinusoidal voltage fields. Top: Input voltage fields used for training and testing followed by performance of various methods in the case of noise-free data. Bottom: Noisy output displacement profiles used for training and testing followed by performance of various methods in the case of 10% Gaussian noise. The solid black curve denotes the predictions, and the dashed red line depicts the ground truth.

considerable distortion, particularly in the mid-region of the loops, indicating a failure to maintain the consistency and continuity of the hysteresis pattern. The results suggest that LSTM struggles with the complexity of the input–output relationship, indicating its limitations in generalization to unseen input voltage profiles.

Similarly, the GRU predictions, presented in Fig. 3(e), are characterized by even greater deviations from the ground truth, with noticeable irregularities in the shape and alignment of the loops. The results collectively suggest that while recurrent neural networks like LSTM and GRU are a natural framework for capturing temporal dependencies, they are not well-suited for modeling the relationship in the case of unseen voltage profiles, indicating their limitations in generalization.

Furthermore, to demonstrate the robustness of the proposed method on real-world problems, the displacement profile is corrupted with additive Gaussian noise with a standard deviation that is 10% of the standard deviation of the noise-free output, as shown in Fig. 3(f). Subsequently, these noisy data are used as the output for training and testing the neural network models. The results presented in the bottom row of Figs. 3(g)–3(j) show that neural operator methods retain their qualitative prediction accuracy even for noisy output data, demonstrating the robustness of the proposed approach.

The tabulated error metrics in Table I underscore the superior performance of FNO and DeepONet in approximating the hysteresis loops. FNO achieves the lowest errors across all metrics in noise-free and noisy data conditions, indicating its accuracy. DeepONet follows

closely with slightly higher errors, still demonstrating robust performance. In contrast, LSTM and GRU models exhibit significantly higher errors in all metrics, reflecting their inability to capture the complex dynamics of the hysteresis loops accurately.

For the second experiment, the considered ODE modeling the butterfly-shaped hysteresis is[2]

$$\dot{d}(t) = 0.8|\dot{v}(t)|v(t)y(t) - 1.7|\dot{v}(t)|d(t)y(t) + 0.5\dot{v}(t)y(t), \quad (8)$$

where $y(t)$ is the output obtained from (4) and the rest of the symbols have their usual meaning. The input voltage fields are generated similarly to those in the first experiment. The hyperparameters for all four methods are the same as in the first experiment.

Figure 4 illustrates the performance of different methods in predicting the butterfly-shaped hysteresis loops. FNO, shown in Fig. 4(a), demonstrates the most accurate predictions, closely aligning with the ground truth across the entire voltage range. The predictions suggest that FNO effectively captures the nonlinear dynamics characteristic of butterfly-shaped hysteresis. In contrast, while DeepONet, shown in Fig. 4(b), performs well overall, it exhibits noticeable deviations in certain regions, indicating some limitations in its ability to generalize across the entire input space. The DeepONet predictions can be further improved through an inductive bias by constraining its outputs to be positive (Constrained DeepONet). This constraint is performed by taking the square of the prediction of DeepONet and using it in the

TABLE I. Errors obtained for various methods in approximating hysteresis loops described by (4) with sinusoidal inputs for noise-free and noisy data. The boldface denotes the least obtained error among the considered methods.

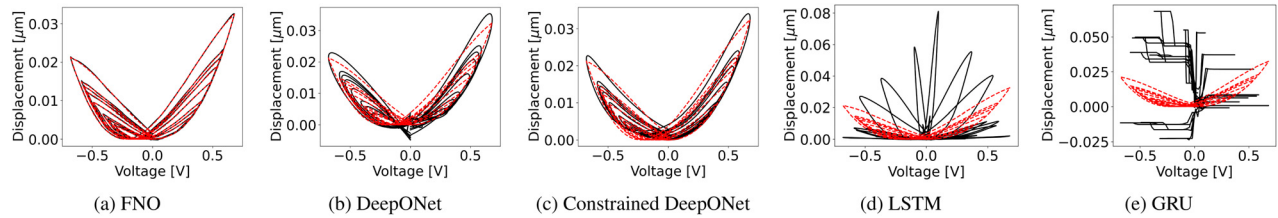| Method	Noise-free			10% Gaussian noise		
	$\mathscr{R}$	MAE	RMSE	$\mathscr{R}$	MAE	RMSE
FNO	$\mathbf{5.62 \times 10^{-3}}$	$\mathbf{4.31 \times 10^{-4}}$	$\mathbf{5.72 \times 10^{-4}}$	$\mathbf{9.98 \times 10^{-2}}$	$\mathbf{6.41 \times 10^{-3}}$	$\mathbf{1.03 \times 10^{-2}}$
DeepONet	5.93×10^{-2}	4.13×10^{-3}	6.09×10^{-3}	1.16×10^{-1}	7.68×10^{-3}	1.20×10^{-2}
LSTM	7.89×10^{-1}	6.15×10^{-2}	8.11×10^{-2}	7.92×10^{-1}	6.16×10^{-2}	8.18×10^{-2}
GRU	7.99×10^{-1}	6.36×10^{-2}	8.21×10^{-2}	8.16×10^{-1}	6.50×10^{-2}	8.44×10^{-2}

FIG. 4. Performance of neural network models in predicting hysteresis loops described by (8) for sinusoidal voltage fields. The solid black curve denotes the predictions, and the dashed red line depicts the ground truth.

TABLE II. Errors obtained for various methods in approximating butterfly hysteresis loops described by (8). The boldface denotes the least obtained error among the considered methods.

Method	$\mathscr{R}$	MAE	RMSE
FNO	$\mathbf{7.73 \times 10^{-3}}$	$\mathbf{1.15 \times 10^{-4}}$	$\mathbf{1.51 \times 10^{-4}}$
DeepONet	9.61×10^{-2}	1.20×10^{-3}	1.88×10^{-3}
Constrained DeepONet	7.64×10^{-2}	8.94×10^{-4}	1.49×10^{-3}
LSTM	1.03×10^{-0}	1.31×10^{-2}	2.03×10^{-2}
GRU	1.07×10^{-0}	1.52×10^{-2}	2.09×10^{-2}

loss function along with the observational labeled data. The result of constrained DeepONet is presented in Fig. 4(c), showing predictions are more aligned to the displacement profiles than vanilla DeepONet.

LSTM and GRU, depicted in Figs. 4(d) and 4(e), respectively, fail to capture the hysteresis behavior accurately, with misaligned predictions. These results underscore the superior efficacy of FNO in modeling complex hysteresis loops while highlighting the comparative weaknesses of LSTM and GRU in such tasks. Table II presents the error metrics for the performed experiment, aligning with the results obtained in the first experiment, with FNO providing the most accurate results and LSTM and GRU failing to capture the dynamic nonlinearity.

For the third experiment, complicated voltage fields are used as inputs in (4) instead of sinusoidal fields to evaluate the potential of the proposed methods further. Specifically, diverse, complex, non-periodic input voltage functions are sampled from a Gaussian process using a radial basis function (RBF) kernel as shown in Fig. 5(a). The RBF kernel has a variance of 1 and a length scale of 0.2 to ensure the generated functions are complex and non-periodic, avoiding simplistic or repetitive patterns. All other hyperparameters are kept the same for all four methods except for the number of epochs, which is ten times that of the previous experiments, to ensure convergence of the training process.
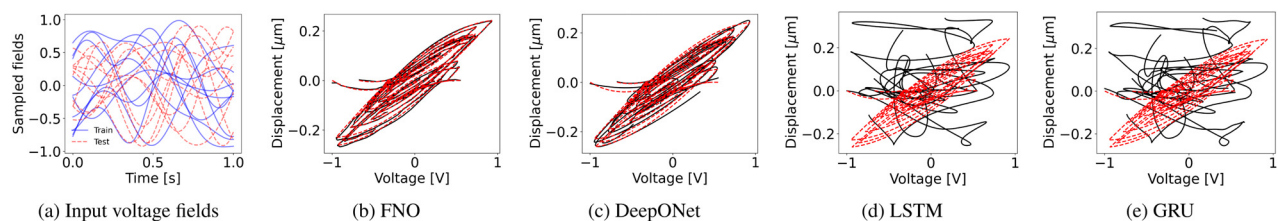
The performance of neural network models in predicting hysteresis loops derived from Gaussian random fields is presented in Fig. 5. The input voltage fields used for training and testing [Fig. 5(a)] are represented with the blue and red curves, respectively. The comparisons of the predictions made by the neural network models against the ground truth are shown in Figs. 5(b)–5(e). The solid black lines in each plot represent model predictions, while the dashed red lines indicate the ground truth. The FNO and DeepONet models in Figs. 5(b) and 5(c) show superior performance, closely aligning with the ground truth. In contrast, LSTM and GRU in Figs. 5(d) and 5(e) showcase their insufficiency in capturing the complex hysteresis behavior. Moreover, Table III presents the error metrics for the performed experiment, aligning with the results obtained in the previous experiments, with neural operator methods providing accurate results and recurrent neural architectures failing to capture the dynamic nonlinearity.

This Letter presented a deep learning approach for modeling hysteresis in piezoelectric materials, namely, neural operators. The study demonstrated that neural operators yield generalizable models, which are crucial in scenarios where prior training on diverse voltage profiles is not feasible. By leveraging prominent operator networks, specifically the Fourier neural operator (FNO) and the deep operator network (DeepONet), the operators robustly predicted hysteresis loops, including the butterfly-shaped hysteresis loops, outperforming conventional recurrent architectures and leading to the development of generalizable neural hysteresis models.

Employing neural operators contributes to neural hysteresis modeling by developing accurate and generalizable models predicting real-time piezoelectric responses. Future research would include exploring and developing further advanced operator training methodologies, including quantifying their performance on real material data. Approaches such as transfer learning,[34] pre-trained network parameters, and meta-learning[35] strategies could be employed to expedite model convergence. In addition, future work will also include

FIG. 5. Performance of neural network models in predicting hysteresis loops described by (4) for Gaussian random fields. Input voltage fields used for training and testing (a) followed by performance of various methods (b)–(e). The solid black curve denotes the predictions, and the dashed red line depicts the ground truth.

TABLE III. Errors obtained for various methods in approximating hysteresis loops obtained on Gaussian random input voltage fields. The boldface denotes the least obtained error among the considered methods.

Method	$\mathscr{R}$	MAE	RMSE
FNO	$\mathbf{4.45 \times 10^{-2}}$	$\mathbf{3.76 \times 10^{-3}}$	$\mathbf{5.46 \times 10^{-3}}$
DeepONet	6.62×10^{-2}	5.90×10^{-3}	8.12×10^{-3}
LSTM	1.43×10^{-0}	1.36×10^{-1}	1.75×10^{-1}
GRU	1.42×10^{-0}	1.42×10^{-1}	1.82×10^{-1}

comprehensive comparisons with the traditional phenomenological models like the Preisach model.

AUTHOR DECLARATIONS
Conflict of Interest

The authors have no conflicts to disclose.

Author Contributions

Abhishek Chandra: Conceptualization (lead); Data curation (lead); Formal analysis (lead); Investigation (lead); Software (equal); Validation (equal); Writing – original draft (lead); Writing – review & editing (equal). **Taniya Kapoor:** Software (equal); Validation (equal); Writing – review & editing (equal). **Mitrofan Curti:** Funding acquisition (equal); Supervision (equal); Writing – review & editing (supporting). **Koen Tiels:** Funding acquisition (equal); Supervision (equal); Writing – review & editing (supporting). **Elena A. Lomonova:** Funding acquisition (equal); Resources (lead); Supervision (equal).

DATA AVAILABILITY

The data that support the findings of this study are openly available in GitHub at https://github.com/chandratue/piezoelectric_hysteresis_neural_operator.

REFERENCES

[1]P. Muralt, R. G. Polcawich, and S. Trolier-McKinstry, "Piezoelectric thin films for sensors, actuators, and energy harvesting," MRS Bull. **34**, 658–664 (2009).

[2]A. Chandra, B. Daniels, M. Curti, K. Tiels, E. A. Lomonova, and D. M. Tartakovsky, "Discovery of sparse hysteresis models for piezoelectric materials," Appl. Phys. Lett. **122**, 214101 (2023).

[3]N. Strijbosch, K. Tiels, and T. Oomen, "Memory-element-based hysteresis: Identification and compensation of a piezoelectric actuator," IEEE Trans. Control Syst. Technol. **31**, 2863–2870 (2023).

[4]F. Preisach, "Über die magnetische nachwirkung," Z. Phys. **94**, 277–302 (1935).

[5]C. Serpico and C. Visone, "Magnetic hysteresis modeling via feed-forward neural networks," IEEE Trans. Magn. **34**, 623–628 (1998).

[6]S. Quondam-Antonio, F. Riganti-Fulginei, A. Laudani, G.-M. Lozito, and R. Scorretti, "Deep neural networks for the efficient simulation of macro-scale hysteresis processes with generic excitation waveforms," Eng. Appl. Artif. Intell. **121**, 105940 (2023).

[7]S. Q. Antonio, F. R. Fulginei, A. Laudani, A. Faba, and E. Cardelli, "An effective neural network approach to reproduce magnetic hysteresis in electrical steel under arbitrary excitation waveforms," J. Magn. Magn. Mater. **528**, 167735 (2021).

[8]F. R. Fulginei and A. Salvini, "Neural network approach for modelling hysteretic magnetic materials under distorted excitations," IEEE Trans. Magn. **48**, 307–310 (2012).

[9]X. Zhang, Y. Tan, and M. Su, "Modeling of hysteresis in piezoelectric actuators using neural networks," Mech. Syst. Sig. Process. **23**, 2699–2711 (2009).

[10]Y. Yu, X. Si, C. Hu, and J. Zhang, "A review of recurrent neural networks: LSTM cells and network architectures," Neural Comput. **31**, 1235–1270 (2019).

[11]J. Lien, A. York, T. Fang, and G. D. Buckner, "Modeling piezoelectric actuators with hysteretic recurrent neural networks," Sens. Actuators A **163**, 516–525 (2010).

[12]L. Deng and Y. Tan, "Diagonal recurrent neural network with modified back-lash operators for modeling of rate-dependent hysteresis in piezoelectric actuators," Sens. Actuators A **148**, 259–270 (2008).

[13]S. Hochreiter, "Long short-term memory," Neural Computat. **9**, 1735 (1997).

[14]K. Cho, B. Van Merriënboer, C. Gulcehre, D. Bahdanau, F. Bougares, H. Schwenk, and Y. Bengio, "Learning phrase representations using RNN encoder-decoder for statistical machine translation," arXiv:1406.1078 (2014).

[15]J. Li, Y. Huang, Q. Li, and Y. Li, "Closed-LSTM neural network based reference modification for trajectory tracking of piezoelectric actuator," Neurocomputing **467**, 379–391 (2022).

[16]Y. Yang, "Hysteresis loop modeling of piezoelectric cantilevered actuators based on LSTM neural network," in *2023 3rd International Conference on Energy, Power and Electrical Engineering (EPEE)* (IEEE, 2023), pp. 1128–1131.

[17]Y. Yang, "LSTM-based hysteresis modeling and PSO-driven compensation for piezoelectric cantilever actuators," in *2023 3rd International Conference on Digital Society and Intelligent Systems (DSInS)* (IEEE, 2023), pp. 32–35.

[18]T. Kapoor, A. Chandra, D. M. Tartakovsky, H. Wang, A. Núñez, and R. Dollevoet, "Neural oscillators for generalization of physics-informed machine learning," AAAI J. **38**, 13059–13067 (2024).

[19]T. Kapoor, A. Chandra, D. Tartakovsky, H. Wang, A. Núñez, and R. Dollevoet, "Neural oscillators for generalizing parametric PDEs," in *Symbiosis of Deep Learning and Differential Equations III* (TU Delft, 2023).

[20]A. Chandra, T. Kapoor, B. Daniels, M. Curti, K. Tiels, D. M. Tartakovsky, and E. A. Lomonova, "Neural oscillators for magnetic hysteresis modeling," arXiv:2308.12002 (2023).

[21]T. Kapoor, H. Wang, A. Núñez, and R. Dollevoet, "Transfer learning for improved generalizability in causal physics-informed neural networks for beam simulations," Eng. Appl. Artif. Intell. **133**, 108085 (2024).

[22]A. Chandra, B. Daniels, M. Curti, K. Tiels, and E. A. Lomonova, "Magnetic hysteresis modeling with neural operators," arXiv:2407.03261 (2024).

[23]K. Azizzadenesheli, N. Kovachki, Z. Li, M. Liu-Schiaffini, J. Kossaifi, and A. Anandkumar, "Neural operators for accelerating scientific simulations and design," Nat. Rev. Phys. **6**, 320 (2024).

[24]Z. Li, N. Kovachki, K. Azizzadenesheli, B. Liu, K. Bhattacharya, A. Stuart, and A. Anandkumar, "Fourier neural operator for parametric partial differential equations," arXiv:2010.08895 (2020).

[25]L. Lu, P. Jin, G. Pang, Z. Zhang, and G. E. Karniadakis, "Learning nonlinear operators via DeepONet based on the universal approximation theorem of operators," Nat. Mach. Intell. **3**, 218–229 (2021).

[26]S. Wang, H. Wang, and P. Perdikaris, "Learning the solution operator of parametric partial differential equations with physics-informed DeepONets," Sci. Adv. **7**, eabi8605 (2021).

[27]Z. Hao, Z. Wang, H. Su, C. Ying, Y. Dong, S. Liu, Z. Cheng, J. Song, and J. Zhu, "GNOT: A general neural operator transformer for operator learning," arXiv:2302.14376 (2023).

[28]Y. Wang, C. Xiong, C. Ju, G. Yang, Y.-W. Chen, and X. Yu, "A deep transfer operator learning method for temperature field reconstruction in a lithium-ion battery pack," IEEE Trans. Ind. Inf. **20**, 8089–8101 (2024).

[29]M. Yin, E. Zhang, Y. Yu, and G. E. Karniadakis, "Interfacing finite elements with deep neural operators for fast multiscale modeling of mechanics problems," Comput. Methods Appl. Mech. Eng. **402**, 115027 (2022).

[30]T. Kapoor, H. Wang, A. Núñez, and R. Dollevoet, "Physics-informed neural networks for solving forward and inverse problems in complex beam systems," IEEE Trans. Neural Networks Learn. Syst. **35**, 5981 (2024).

[31]N. S. Ottosen and M. Ristinmaa, *The Mechanics of Constitutive Modeling* (Elsevier, 2005).

[32]D. P. Kingma, "Adam: A method for stochastic optimization," arXiv:1412.6980 (2014).

[33]X. Glorot and Y. Bengio, "Understanding the difficulty of training deep feedforward neural networks," in *Proceedings of the Thirteenth International Conference on Artificial Intelligence and Statistics* (JMLR, 2010), pp. 249–256.

[34]F. Zhuang, Z. Qi, K. Duan, D. Xi, Y. Zhu, H. Zhu, H. Xiong, and Q. He, "A comprehensive survey on transfer learning," Proc. IEEE **109**, 43–76 (2021).

[35]R. Vilalta and Y. Drissi, "A perspective view and survey of meta-learning," Artif. Intell. Rev. **18**, 77–95 (2002).